RSC Advances

ROYAL SOCIETY OF CHEMISTRY

www.rsc.org/advances

Graphical abstract

ZnONPs was synthesized using ferulic acid as reductant and intricate bifold role as DNA binder and radio sensitizer were reviled, which can pave way for anticancer therapy.

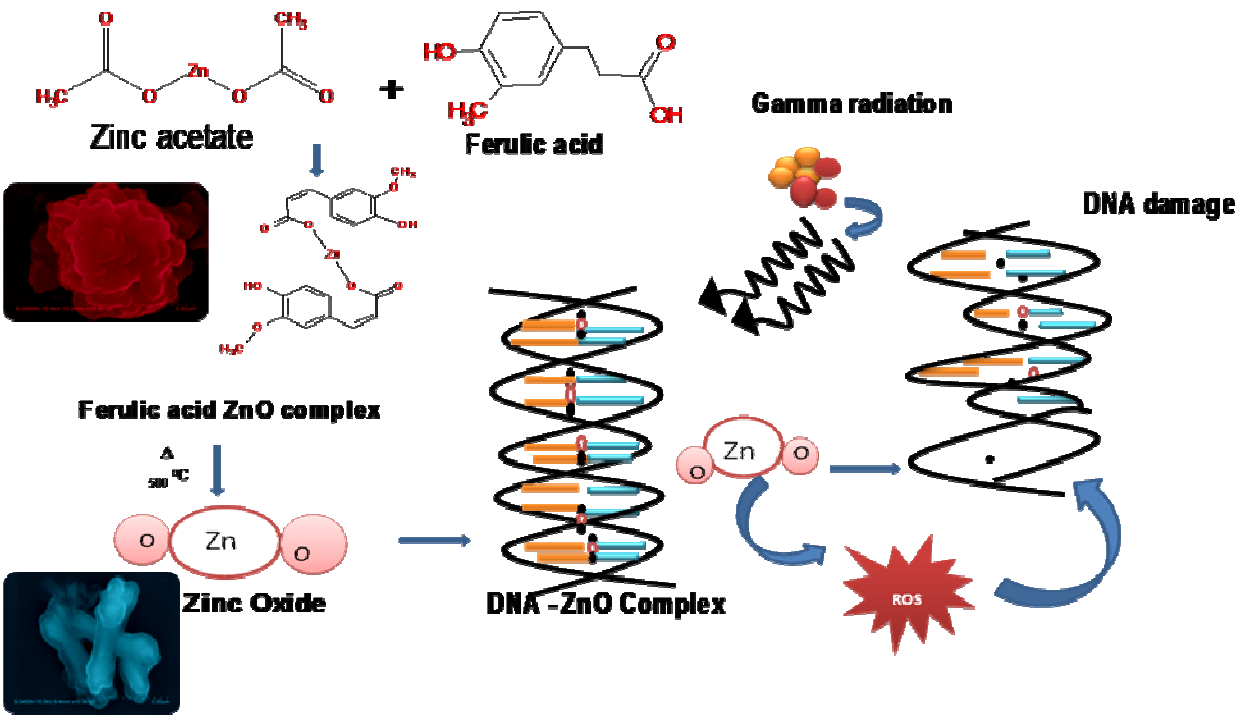

Extracellularly synthesized ZnO nanoparticles interact with DNA and augment gamma radiation induced DNA damage through reactive oxygen species

E. Preedia Babu[a], A. Subastri[a], A. Suyavaran[a], P. Lokeshwara rao[a], M. Suresh Kumar[b], K. Jeevaratnam[a], and C. Thirunavukkarasu[a,c*]

[a] *Department of Biochemistry and Molecular Biology, Pondicherry University, Puducherry 605 014, India.*

[b] *Centre for Bioinformatics, Pondicherry University, Puducherry 605 014, India*

[c] *Present Address: Department of Medicine - Gastroenterology and Liver diseases, 625, Ullmann Building, Albert Einstein College of Medicine of Yeshiva University, Bronx, NY 10469*

* *Corresponding author: Tel.:+91 413 2654972 or* +011 347 471 6477*; Fax: +91 413 2655255; E-mail address: tchinnasamy@hotmail.com (C.Thirunavukkarasu)*

ABSTRACT

The present study brings a green synthesis of highly stable and biocompatible ZnO nanoparticles (ZnONPs) using ferulic acid as reductant. The biosynthesized nanoparticles were characterized by UV-visible spectroscopy, photoluminescence spectroscopy, X-ray diffraction, Raman spectroscopy, Fourier transform infrared spectroscopy, thermo gravimetric analysis, differential scanning calorimetry, scanning electron microscopy, atomic mass spectroscopy, energy dispersive X-ray spectroscopy and elemental mapping. The characterization results elucidates the formation of crystalline wurtzite structured acicular shaped ZnONPs. Further the intricate mechanism of ZnONPs – DNA interaction was studied. The binding affinity and mechanism of ZnONPs with Calf thymus-DNA interactions were scrutinized and conformational changes were analyzed. The result reveals interaction of ZnONPs with DNA in intercalation mode and the values of binding constant (K) and Stern-Volmer quenching constant (Ksv) were found to be 5.8×10^{5} M^{-1} and 4.1×10^{5} M^{-1} respectively. Furthermore gamma radiation induced reactive oxygen species (ROS) generation and DNA damage by ZnONPs were analyzed by various spectrophotometric methods, which unveiled the radiosensitizer role of ZnONPs through significant increased generation of ROS. Our current experimental evidence explores the ZnONPs dual role capacity as DNA binder as well as radiosensitzer. Based on present research findings we conclude that ZnONPs can be gifted anticancer agent, warranting *in vivo* studies.

Keywords:

ZnO nanoparticles, DNA interaction, DNA damage, Gamma radiation, Spectroscopy

1. Introduction

Nanomaterials play a relevant role in the development of biosensors, nanomedicines, clinical diagnostics, and chemotherapeutics.[1-4] Until recent years, scientists were attracted on metal oxide based nano-particle synthesis, as they proved its competence in all fields of science because of its unique chemical, physical and multifunctional properties. Among the metal oxides, zinc oxide nanoparticles (ZnONPs) is considered as promising candidate in metal oxide nanoparticle, due to its biocompatibility it is used in drug delivery, bioimaging, antibacterial and antifungal activity.[5, 6] As zinc serves as a co factor for various enzymes, it holds a key role in regulation of various metabolic pathway, further it has been used as folk remedy for various disorder including wound healing.[7] It also suppresses sebaceous secretions of skin, and protects from UV rays which makes it a common chemical ingredient in cosmetics. The biomedical importance of ZnONPs is strengthened by recent findings showing its antioxidant, anti-inflammatory, anti-diabetic, anti-proliferative and apoptotic effect.[8-10]

Commonly, ZnONPs can be synthesized by chemical, physical and biological methods. Among these chemical and physical methods like micro emulsion, sono-chemical, sol-gel, polyol, pyrolysis, precipitation by chemicals etc., have some disadvantages like unaffordable cost, requirement of high pressure and energy etc.,[11] Most of these methods use surfactants like sodium dodecyl sulfate, cetyl trimethylammonium bromide etc., for stabilization and prevent re-aggregation. These substances were adsorbed to the surface of nanoparticles which leads to adverse effect on biological system. Except these surfactants, some of the metallic precursors and by products of chemical synthesis also pose chemical toxicity. Green biosynthesis of ZnONPs has gained preference over other conventional synthetic methods as they are simple, lucrative, innocuous, eco-friendly, highly stable, less time consuming and curb the use of high energy and pressure.[6] Green synthesis of nanoparticles is a bottom up method which exploits bioreductants such as phytochemicals and enzymes from plant, bacteria,

fungi, and algae for reduction of the metal complex to respective nanoparticles.[12]Among these, nanoparticle synthesis through microorganism were risky due it's pathogenicity, e.g., *F. oxysporum*[13] and it needs a long procedure for micro organism culture, maintenance and purification.[14] All these qualities make plant based green synthesis as a major focus of nanoparticle synthesis. Though the crude plant extracts are used in green synthetic approach, usage of pure phytochemical is preferred due to its lack of toxicity and improved efficiency. In the present study, from the green perspective a pure phytochemical ferulic acid, which is commonly present in the commenlide plants, was selected as bioreductant and stabilizing agent for ZnONPs preparation. Ferulic acid is one of the health promoting phenolic phytochemical combined with anti-diabetic, anti-inflammatory, antiviral, immune enhancing, antioxidant, neuroprotective and metal chelating activities.[15]Additionally, ferulic acid plays a vital role in the induction of apoptosis by inhibiting anti-apoptotic proteins, suppression of proliferation and metastasis.[16]

Molecular interactions between nanoparticles and DNA are of paramount importance for the development of new nano-based salutary chemotherapeutic drugs.[17] The interacted nanoparticles alter the bio-properties of DNA and DNA binding proteins.[18] It also changes the conformation of DNA, which adversely affects gene expression, replication, repair, transcription and signaling mechanism organized by DNA.[19] So DNA-nano interaction is considered as one of the immersive escalating investigation area under targeted therapies. The efficacy of targeted therapy can be enhanced by combination therapy. Gamma radiation is one of the physical agents used for radiotherapy, for effective elimination of cancer cells, radiotherapy is combined with cytotoxic drugs.[20] Enhancement of radiotherapy is intensified with radiosensitizers. Since, most of the nanoparticles has rediosensitization property, it could be employed as a radiosensitizers to improve the efficiency of radiotherapy. Since most of the nanoparticles has rediosnsitization property[21], ZnONPs could be employed as a

radiosensitizers to improve the efficiency of radiotherapy. To our knowledge the role of biosynthesized ZnONPs as radiosensitizer is not known till date.

In the current study, biomimetic synthesis of zinc oxide nanoparticles and some facet of Calf thymus-DNA (CT-DNA) – ZnONPs interaction and enhancement of gamma radiation induced DNA damage by ZnONPs were of interest.

2. Materials and methods

2.1 Preparation of ZnO nanoparticle

Zinc acetate ($Zn(CH_3COO)_2.2H_2O$, 98%, Himedia) and ferulic acid ($C_{10}H_{10}O_4$, 98%, Sisco Research Laboratories Pvt. Ltd.,) were used as substrate for ZnONPs synthesis. 6 mM of zinc acetate and 12 mM of ferulic acid were made in ethanol. The ferulic acid solution was added to zinc acetate solution. A white homogenous dispersion was obtained, which was incubated at room temperature for 24hr. The precipitate was centrifuged at 6000 rpm for 10 min, washed 3 times with MilliQ water and the final product was dried at room temperature and calcinated at 500°C for 1hr.

2.2 Characterization of the prepared ZnO nanoparticle

The formation and purity of ZnONPs were examined by various characterization methods. The optical absorption spectra of ethanol dispersed ZnONPs before and after calcination were characterized by Shimadzu 1800 UV-visible dual beam grating spectrophotometer. The absorption spectra of diluted solutions were recorded in the wavelength range of 200 to 800 nm at room temperature, ethanol was used as blank. The photoluminescent emission (PL) spectra of ZnONPs were recorded by using JY fluorolog- FL3- 11 spectrofluorometer assembled with single grating monochromator and 450 W xenon

lamps. The PL spectra were measured with 2 nm slit width and an excitation wavelength of 325 nm. Lattice dynamics and crystalline quality of ZnONPs were determined under Raman spectroscopy by Reneishaw spectrometer (NRS-3100), with 514 nm argon ion laser as an excitation source and total incident laser power 30 mW.

Shape and vibrational modes of the functional group of the compounds were analyzed by IR spectra on Fourier transform infrared spectroscopy (FTIR) (Thermo Nicolet 6700:S) in transmission mode, 400–4000 cm^{-1} mid infrared region. Samples were prepared in the form of KBr pellets in which 1 mg ZnONPs crushed with 100 mg KBr and KBr alone were used for reference. The crystalline forms or phases of compound in the calcinated and noncalcinated sample were examined under, Rigaku ultima IV X-ray diffractometer (XRD). The powdered sample was scanned in the diffraction angle range $10^{o} \leq 2\theta \leq 80^{o}$. The average size of the particles was determined by Debye–Scherrer formula, $D = (0.9\lambda) / (\beta \text{ case } \theta)$ in this equation diameter of crystallites are (D), λ denoted the wavelength of CuKα radiation (λ = 1: 5408 Å), θ signifies the Bragg angle, β is full-width at half- maximum in radians (FWHM). A combination of scanning electron microscopy with energy dispersive X-ray spectroscopic technique, Hitachi (S-3400N) were used to analyze the size, surface morphology, elemental composition and purity of the nanoparticles. The prepared ZnONPs suspension was first sonicated and then a drop of the diluted sample was loaded on an aluminium foil coated sample holder followed by its coating with carbon in ultra vacuum. After complete drying in the ultra vacuum, measurements were taken.

Thermal stability and the energy change associated with the transition of ZnONPs were assessed by thermogravimetric analyzer TA instruments Q 600 SDT and Q 20 DSC within the temperature range of 0 – 700ºC, 10 mg of sample were kept in a platinum crucible and the applied heat was 10ºC/min. In this

study, the ethanol dispersed freshly prepared samples of nanoparticle suspension were applied to a glass slide (1×1cm) and air dried for 3 hours so that they form a thin film over the glass slide. The dried film was scanned by atomic force microscope (AFM) (Bruker multimode-8) in tapping mode, using the nanoprobe cantilever made of silicon nitride with a spring constant of 49 Nm^{-1}.

2.3 Studies of CT- DNA– ZnO nanoparticle interaction

2.3.1 Preparation of ZnO nanoparticle dispersions

ZnONPs stock solution (10 mg/ml) in 10 mM Tris HCl (pH 7.5) (Himedia, USA.) buffer was prepared by sonication using a Branson digital sonicator for 20 min in 60% pulsation mode and with a sonication power of ≈60 W after sonication the sample was filtered by 0.2 µm pore size syringe filter. ZnONPs 10, 30 and 50 µg/ ml were used for interaction and DNA damage study.

2.3.2 Preparation of CT-DNA stock solution

Sodium salt of double stranded CT-DNA d(CGCGAATTCGCG) was purchased from Sigma Aldrich India, it consists of ~ 13,000 base pairs. Stock solutions of CT- DNA (10 mg/ml) were prepared in 10 mM Tris HCl buffer at pH 7.5 with gentle shaking until formation of homogenous solution and was stored at 4ºC. The final concentration of CT-DNA was examined by UV-Visible spectrophotometer at 260 nm employing the molar extinction coefficient 6600 cm^{-1}, which was found to be 33.97mM. Furthermore, the 260/280 ratio of CT-DNA was 1.8 which clearly revealed that purity of DNA without any protein contamination.

2.3.3 Interaction studies

The variation of the transmission spectrum of CT-DNA- ZnONPs complex was scrutinized. The absorbance measurement was examined on Shimadzu 1800 spectrophotometer within the wavelength

region of 200–800 nm a 1cm path length rectangular quartz cuvette. For this study varying concentration of ZnONPs were added to the constant concentration of CT-DNA (0.1 mM). The mode of ZnONPs binding to DNA was found out from the analysis of absorbance data, using the well known equation.[22]

$$A_0/A - A_0 = \varepsilon_D/ \varepsilon_{DA} + \varepsilon_D/ (\varepsilon_{DA} .K) \times 1/C_A$$

Where A_0 is the absorbance of pure DNA alone and A is the absorbance of DNA with ZnONPs at 260 nm, ε_D and ε_{DA} are the molar extinction coefficient of pure DNA and DNA- ZnONPs complex, C_A is the concentration of ZnONPs. The binding constant can be calculated by using double reciprocal plot of $1/A- A_0$ Vs $1/C_A$. DNA binding proclivity and stoichiometry of ZnONPs were studied by steady state fluorescence and ethidium bromide (EtBr) competitive displacement assay. In steady state fluorescence assay differing concentration of DNA (0-100 μM) were added to constant concentration of ZnONPs (30 μg/ml). The samples were excited at 325nm, slit width at 2nm and emission spectrum were scanned at 350 to 550nm. The fluorescence intensity was calculated by Stern-Volmer Equation[23], Which is consider as the measure for efficiency of fluorescence quenching by DNA.

$$I/ I_0 = 1+ Ksv [Q]$$

I/I_0 are the ratio of fluorescence intensity in the absence and presence of DNA, Ksv Stern-Volmer quenching constant, and [Q] is the concentration of DNA, further for studying quenching mechanism bimolecular quenching constant Kq was calculated.

$$Kq = Ksv/ \tau$$

τ is the life time of flurophore (10^{-8}). The EtBr displacement assay were carried out using the intercalative agent EtBr (5μM) were mixed with 0.1 mM DNA in Tris HCl buffer of pH 7.5, then ZnONPs (10, 30 and 50 μg/ml) were added to the DNA-EtBr complex. The EtBr emission spectra were measured in the excitation, emission wavelength range of 525 nm and 650 nm respectively. The structural disparity of DNA due to the binding of ZnONPs was monitored by Jasco circular dichroism

spectrometer with a scan speed of 50 nm/min. The spectra of varied concentration of ZnONPs with 0.1 mM CT-DNA in 10 mM Tris-HCl (pH 7.5) were measured in 200–320 nm range in a rectangular quartz cell. Autolab type electrochemical analyser (PGSTAT–302N) was used for cyclic voltammetry. It contains three electrodes, reference, working and the counter electrodes were Ag/AgCl, glassy carbon electrode and platinum (Pt) respectively. The interaction was studied by stepwise addition of DNA to ZnONPs with scanning rate at 100 mV/ Sec.

2.4 Enhancement of gamma radiation induced DNA damage by ZnO nanoparticle

2.4.1 Gamma irradiation

Gamma irradiation was performed in Co-60 gamma chamber GC 5000, at a dose rate of 69.3 Gy min^{-1} for a total dose of 3.068 kGy.[24] The 0.1 mM CT-DNA and DNA- ZnONPs (10, 30 and 50 µg/ml) complex were incubated at 37ºC for 45 min before irradiation.

2.4.2 DNA damage study

UV absorption study of gamma irradiated DNA and DNA- ZnONPs complex were detected within the wavelength range of 200-280 nm by using Shimadzu 1800 spectrophotometer. Fluorescence spectra were analyzed by Fluorolog-FL3-11 spectrofluorometer, after irradiation 5µM EtBr were added to CT-DNA–ZnO complex and the spectra were analyzed the emission wavelength at 600 nm with an excitation at 520 nm. The conformational variation of CT-DNA- ZnO complex due to gamma radiation was monitored by Jasco circular dichroism spectrometer with a scan speed of 50 nm/min. The spectra of varied concentration of ZnONPs with 0.1 mM CT-DNA in 10 mM Tris-HCl (pH 7.5) were measured in 200-320 nm range in a rectangular quartz cell. The ROS generated by gamma radiation were detected by 2, 7 dichlorohydrofluresceindiacetate (DCFDA), 5 mM DCFDA was added to CT-DNA-

ZnONPs complex after gamma irradiation and incubated for 1hr, and the fluorescence were measured by Fluorolog- FL3- 11 spectrofluorometer with an excitation at 495 nm and emission at 520 nm wave length. Furthermore defect formation on ZnONPs were analysed after gammaradiation by Fluorolog-FL3- 11 spectrofluorometer with an excitation at 325 nm.

3. Results and Discussion

Biological method of ZnONPs was prepared by using pure ferulic acid and zinc acetate as precursor. Our method of biosynthesis was eco friendly, simple and without complex machinery. The possible mechanism of synthesis is shown in Fig.1. which may involves the reducing and chelating property of ferulic acid. It forms cationic interaction with Zn^{2+}, where deprotonated carboxylate group of one ferulic acid molecule and hydroxyl group of another ferulic acid molecule helps in the chelation and formation of superstructure of ZnO. Similar mechanism are proposed for reduction of Cu^{2+}.[25] Calcination helps to dissolve the chelation and releases more crystalline ZnONPs.

3.1 Synthesis and confirmation of ZnO nanoparticle formation

The formation of ZnONPs assayed by UV-spectroscopy. Ultraviolet-visible excitation spectra of before and after calcination samples are shown in supplementary Fig. 1. Before calcination spectra has shown 3 peaks (supplementary Fig. 1a) at 215 nm, 287 nm and 310 nm, which indicates the absorption spectra of intermediate complex of ferulic acid, ZnO and Zn-ferulate complex.[26] After calcinations the maximum absorption peak (supplementary Fig. 1b) was obtained at 375 nm confirming the presence of ZnONPs, further blue shifted 5 nm from bulk ZnONPs spectra occurs at 380 nm, this phenomenon attribute the quantum confinement effect.[27] Earlier studies have reported similar absorption peak of

wurtzite hexagonal ZnONPs at 373 nm. These observations confirmed the formation of ZnO nanocrystals after calcination.

PL spectra of ZnONPs reveals the luminescent properties, extrinsic and intrinsic structural defects present in the synthesized ZnONPs. PL spectra of ZnONPs depicted a peak at 418 nm before calcination which is a characteristic excitation peak of single ionized ferulic acid and it attributed to zinc vacancy also (Supplementary Fig. 2a.).[28] After calcination it exhibits strong UV emission at 396 nm and weak fluorescence emissions in visible region which implies band edge absorption and the formation of crystalline ZnONPs after calcination (Supplementary Fig. 2b). Weak blue emission at 410 nm corresponds to zinc vacancy and emission at 450 nm, which occurs due to the transition between shallow donors to valence band (oxygen vacancy), 466 nm indicate oxygen and zinc vacancy or interstitials, 481 nm emission peaks due to transition between the oxygen vacancy and interstitial oxygen, and 492 nm green emissions by oxygen vacancy. These are the effects of recombination of electrons and defective holes. [29]

Raman spectrum relies on in-elastic scattering of monochromatic light, the change in frequency of photons (shifted up or down) by interacting with molecule is compared with original frequency of the molecule which is referred to as Raman effect, it's given the phase, purity, crystalline structure and defect in the molecule.[30] Earlier studies reported that wurtzite (hexagonal) structure having nanoparticle belongs to the C^4_{6v} space group with four atoms per primitive cell.[31] Eight sets of optical phonon are present in ZnONPs, in this A_1, E_1 are infrared Raman active polar mode, they are again classified into transverse optical (A_1T and E_1T) and longitudinal-optical (A_1L and E_1L) and E_2 is the non polar Raman active mode which is split to occupy the C_{3v} sites. Raman spectra from the present study before calcination (Fig. 2a), peaks obtained at 1604 cm^{-1}, 1638 cm^{-1}, 1267 cm^{-1}, 985 cm^{-1}, indicate the

presence of Zn-ferulate complex [26], after calcinations (Fig. 2b) showed a sharp peak at 437 cm^{-1}, which represents Raman active phonon mode, another peak at 333 cm^{-1}, represents second order scattering from E_2 high-E_2 low, it concluded that the exact active mode of Raman represents a perfect crystalline ZnO structure with less defects.[32] The stretching vibrations of functional moieties of the molecule with respect to infrared radiation were determined by FTIR (Fig. 3 a&b). The IR spectrum with the peaks at 3405 cm^{-1} and 2361 cm^{-1} (carboxylic O-H stretching), 2842 cm^{-1} (C-H stretches) 1640 cm^{-1} and 1601 cm^{-1} (aromatic C=C stretching), 1265 cm^{-1}, 1216 cm^{-1}, 1157.4 cm^{-1} (carboxylic acid C-O stretching) and 1510 cm^{-1} 1605 cm^{-1}(aromatic C=C) confirms the skeleton of ferulic acid [33] and a narrow peak at 434.9 cm^{-1}, represent the characteristic peak of ZnONPs which corresponds to Raman active E_2 phonon. After calcination a narrow band at 449 cm^{-1} corresponds to stretching vibration of ZnONPs, other small bands, 979 cm^{-1}, 583 cm^{-1}, etc., are due to carbon moiety because of air.[34] These results confirm the formation of Zn-ferulate complex before calcination and after heat treatment it release ZnONPs.

3.2 Characterization of ZnONPs

Crystalline structure of synthesized calcinated and non-calcinated ZnONPs were characterized by X- ray diffractometer. Curtail peaks were procured before calcinations (Fig. 3c) and narrow, intense peaks after calcinations showed in Fig. 3d. This change in nature of peaks signifies increased nanocrystallites in the sample due to calcinations. The peaks at 2θ = 31.99°, 34.34°, 36.39°, 47.40°, 56.55°, 62.81°, 66.5°, 67.90°, 69.24°, 72.62°, and 77. 03° were assigned to (100), (002), (101), (102), (110), (103), (200), (112), (201), (004), (202) of ZnONPs, indicating that the samples were polycrystalline hexagonal wurtzite structure with lattice constant at a = 0.3247, c = 0.5203 same as a pure compound (Zincite, JCPDS 98-006-5172, Fig. 3e). Scherrer formula was used to calculate the average size of the particle and was found to be 31 nm (Table 1). The surface morphology of the

287 synthesized nanoparticle was characterized by scanning electron microscope. The signals of secondary
288 electron produced by the interaction of the external electron beam with electrons on the surface of
289 sample were analyzed. 3D image of ZnONPs with 3 μm, magnification showed a small acicular shaped
290 and got aggregated to form flower like structure (Fig. 4a&b). Chemical characterization of ZnONPs
291 was done by energy dispersive X- ray spectroscopy (Fig. 5). Electrons from the inner shell of the
292 sample which were ejected by a high energy incident electron or x-ray beam, which results in the
293 generation of hole inside the atom to be filled by electron from higher energy shell, the energy
294 difference between higher and lower energy shell producing X- ray line.[35] The intensity of zinc peak of
295 calcinated sample was higher than before calcinations (Fig. 5a), the spectrum shown in Fig. 5b has six
296 absorption peaks, between them three are zinc peaks, two are from K shell and one L shell, one from
297 oxygen, while the carbon peak is from carbon coating and peak of Al from aluminium foil used as
298 substrate.[36] No other elemental peaks were observed, indicating the purity of ZnONPs. Spatial
299 distribution of elements were scrutinized by elemental mapping (Figure 5c-f), the results imply uniform
300 distribution of zinc and oxygen. Intensity of zinc distribution increased after calcinations.[37]
301
302 The thermal characteristics were analyzed by thermogravimetry-differential thermal analysis
303 (TG-DTA) and differential scanning calorimetry (DSC). The TG-DTA result reveals that before
304 calcinations (Supplementary Fig. 3a) greater mass loss has occurred in the temperature range of 265ºC
305 to 375ºC, (19.3%) it continues upto 600ºC, (53.28%). But after calcinations (Supplementary Fig. 3b)
306 weight loss occurs up to 300ºC, which was only 6.42%. DSC peak of the sample before calcination has
307 one endothermic peak at 281ºC which indicates the product of catalysis and one exothermic peak at
308 363.58ºC. But, after calcinations only a single exothermic peak at 373ºC was found. The result
309 indicates that after calcinations quality and thermal stability of ZnONPs were improved.[38] The three
310 dimensional surface contour of ZnONPs was analyzed by atomic force microscopy and the results are

depicted in Fig. 6. The size, shape, height distribution and roughness of the surface of ZnONPs were clear in the 3D structure. The sample before calcination had surface, rougher than sample after calcination. Size of the nanoparticles was in 15-20 nm range, shape was acicular and height distribution was found to be around 8.8 nm and 23.5 nm. These results indicated that after calcination pure crystalline, highly stable ZnONPs was obtained, [34] which were used for further CT-DNA interaction and gamma radiation induced DNA damage.

3.3 CT- DNA – ZnO nanoparticle interaction studies

The UV–visible absorption spectra of CT-DNA and ZnONPs complex are shown in Fig. 7a. The CT- DNA shows maximum absorption at 260 nm because of the electronic transition occurs in chromophoric groups present in pyrimidine and purine components. The absorbance of CT-DNA was gradually decreased at 260 nm with red shift while increasing the concentration of ZnONPs. This decreased absorbance signifies π-π^* stacking interaction between ZnONPs and the base pair of DNA, this stacking interaction lowering the transition energy which leads red shift.[39] During stacking interaction, the π^* orbital of ZnONPs was partially filled by electrons which decrease the probability for transition which cause hypochromic effect. This hypochromic effect with red shift of UV spectrum clearly revealed that ZnONPs binds with DNA through intercalating mode.[40] This result agree with the previous theoretical findings.[41] The binding constant of the nanoparticle and DNA complex was determined from the slope and intercept of the linear graph as 5.8×10^5 M^{-1} which binding constant value shows strong interaction between ZnONPs and CT- DNA when compared to classical intercalator such as riboflavin.[42]

The sensitivity and selectivity of fluorescence emission spectroscopy makes it a commonly using tool for the interaction studies. The molecular interactions such as molecular rearrengements,

energy transfer, excited – state reaction and complex formation, may leads to decreased fluorescent intensity this process is known as quenching.[43] In steady state fluorescence, the emission spectrum of ZnONPs showed (Fig 7b) a broad emission peak at 423nm, by increasing concentration of DNA the fluorescence intensity enhanced with a short hypsochromic shift which indicated the strong interaction of ZnOPs with DNA which diminishes the quenching property of DNA[44.] For finding the mode of interaction, the ratio of fluorescence intensity in presence and absence of DNA (F/F_0) has been plotted as a function of DNA concentration, the plot showed a linear relationship between fluorescence intensity and DNA concentration. The efficiency of fluorescence quenching by DNA was calculated by Stern – Volmer quenching constant (Ksv) from the slop of F/F_0 Vs [Q] plot, the value was found to be 4.1×10^5 which was similar to the other intercalators.[45] For studying the type of quenching mechanism bimolecular quenching constant Kq was calculated which is 4.1×10^{13}. Commonly, two main types of quenching mechanism which are dynamic quenching and static quenching this can be assessed by comparing Kq value with bimolecular limiting diffusion rate constant 2×10^{10}, if the value of bimolecular quenching constant is found to be greater than limiting diffusion rate constant, then the quenching process is static, in case of dynamic quenching it should be lesser than Kq value. The present study it would be static quenching so that the distance between the ZnO NPs and DNA must be < 20A° [46] It might be due to the formation of ground state complex of intercalated ZnONPs with DNA.[47] To conform the intercalator mode of interaction EtBr displacement assay were carried out. The flurophore EtBr has strong intercalation between the base pairs of DNA and emits intense fluorescence in the presence of DNA at 606 nm when excited at 520 nm. The Fig. 7c shows the addition of ZnONPs (10, 30, 50 µg/ml) the fluorescent intensity of DNA-EtBr complex gets decreased, which implies the displacement of intercalating agent by ZnONPs. which shows competitive interaction between ZnONPs and EtBr for the binding site and gives a good agreement about the strong intercalative binding of ZnONPs with DNA.[48]

Circular dichroism study was performed to investigate the conformational change of DNA due to binding of ZnONPs. There are four marker band for B form of DNA, i.e. at 210 nm (negative), 220 nm (positive), and 245 nm (negative) due to base stacking and 281 nm (positive) due to, helicity of B - DNA conformation (Fig. 8a). [49] The conformational changes are analyzed by the position and intensity of these bands, during the transition from B to Z form of DNA has a negative band around 290 nm, a positive band at 260 nm [50] and a transition from B to A form a decrease band intensity at 210 nm, increased intensity at 280 nm, and a shift occur to higher wavelength at 220 nm.[51] When increasing concentration of ZnONPs (10, 30, 50 µg/ml) is added in to the DNA containing buffer, DNA – ZnONPs complex were formed and there was a gradual decrease in positive and negative bands intensities without any significant shift of the band peaks. This change emphasizes that B form of DNA has no conformational change to A or Z form but slight destacking of DNA base pair occurs due to ZnONPs interaction, and thus leads to changing the conformation from B to C form.[52]

Electrochemical property of ZnONPs–DNA complex was analyzed by cyclicvoltammetry with a potential range from -0.6 V to 1.2 V (Fig. 8b). The result shows that in absence of ZnONPs, cathodic peak at 0.2418 and anodic peak at 0.081, peak potential difference was found to be 160 mV which indicates electrochemical reaction coupled chemical reaction. Upon step wise addition of ZnONPs peak potential shifted to positive direction, ΔE^0 value shifted to negative direction and peak current was decreased, it implies intercalation of ZnONPs between the stacked base pair of DNA.[53]

3.4 Enhancement of gamma radiation induced DNA damage by ZnO nanoparticle

DNA damage due to gamma radiation was appraised by the reflection or transmittance property of DNA alone and DNA- ZnONPs complex by spectrophotometry. The result (Supplementary Fig. 4) showed that due to gamma radiation the absorbance of ZnONPs–DNA complex has increased gradually than before radiation, this may be due to radiation of ZnONPs separate the double stranded DNA, consequently reduced base pair interaction leads to increased UV absorption. The damage of secondary structure of DNA leads to hyperchromicity. It elucidates that gamma radiation had inflicted damage to the DNA helix and ZnONPs intercalation has enhanced the damage. [54]

Gamma radiation induced DNA damage was confirmed by spectrofluorimetry by using EtBr as a fluorescent probe for DNA (naturally weak fluorescence emission). [24] EtBr is a strong intercalating agent and emission intensity of DNA is increased in the presence of EtBr but after gamma radiation (Fig. 9) the fluorescence intensity decreased by increasing the concentration of ZnONPs (10, 30, 50 µg/ml). This signifies that gamma radiation induces DNA damage in double helix, hence excess EtBr left over in the solution, leads to relative decrease in the fluorescence intensity.[55] Fluorimetric estimation results of samples before radiation and after radiation were compared which indicates a larger decrease in fluorescence intensity after gamma radiation.

The conformational change of DNA-ZnONPs complex after irradiation was assessed by circular dichroism spectrum Fig. 10. As it occurred before radiation, a characteristic B conformation appeared with a positive peak at 281 nm and a negative peak at 245 nm. But there is an increase in the intensity of positive and negative peak and the positive peak shifted from 280 to 270 nm. The increase in positive peak intensity was more when compared to the before radiation peak intensity. This

comparison result implies that gamma radiation of ZnONPs–DNA complex leads to more destacking and unwinding of double stranded DNA .[56]

Formation of reactive oxygen species (ROS) in gamma radiation induced DNA-ZnONPs complex were analyzed by using DCFA, which is a fluorescent probe for ROS. It is detected by fluorescent spectroscopy with excitation at 503 nm and an emission peak observed at 520 nm.[57] This result (Fig. 11) signifies the generation of ROS in negative control (buffer alone) that occurs by radiolysis of the buffer, but the intensity of ROS generated is very less when compared to ZnONPs–DNA complex. This significant amount of ROS generation in ZnO- DNA complex may be due to the activation of defect present in ZnONPs through gamma radiation which leads to oxidative damage in DNA.

Furthermore, the defect formation in gamma radiated and non-gamma radiated ZnONPs were analyzed by using fluorescence emission spectroscopy and results were represented in supplementary fig 5. Generally in fluorescence emission study, ZnO has shown two emission peaks such as UV emission peak present at below 400nm and broad green emission peak present at above 400nm. In our current study, gamma radiated ZnONPS exhibited decreased intensity in total number of peaks present on ZnONPS as compared to non gamma radiated sample however, the gamma radiated ZnONPS shows increased intensity in UV emission peaks when compared to the green emission peak of intensity. This may indicates the oxygen vacancies of ZnONPS lattice,[58] which leading to the formation of electron-hole pair which splits water molecule into H^+ and OH^-. This hydroxyl radical inflicts severe oxidative damage to DNA, which may leads to lethal complications of the target cell/organ.[59] Conclusively, the ZnONPs might be encourage gamma radiation induced DNA damage in cancer cells.

4. Conclusions

In summary, a green synthetic approach was employed for synthesis of bio- benign ZnONPs by using ferulic acid as a reductant. The size and structural properties of ZnONPs were analyzed by different characterization techniques. The result implies crystalline wurtzite structured ZnONPs were obtained and size of the nanoparticle lies between 20-30 nm as attested by AFM and X-ray diffraction crystallography. Furthermore, the synthesized nanoparticle was explored for DNA interaction and radiosensitizer role. The CT-DNA interaction studies were evaluated using photoluminescence and UV-visible spectroscopy and it reveals high affinity in intercalative mode of interaction with CT-DNA. Conformational changes were analyzed by CD spectroscopy indicate no characteristic change of B form to A or Z but, base pair unstacking was noticed. It was also found that the electrochemical characteristics support the intercalative mode of interaction. Exposure to gamma radiation, generates ROS in CT-DNA/ZnONPs complex leading oxidative DNA damage which was analyzed by UV visible and fluorescence spectroscopy. The advantage of present biological method of synthesis is simple, easy, and eco-friendly. Moreover, DNA-ZnONPs interaction is a promising aspect in the field of pharmacokinetics for various biomedical applications. As a radiosenzitiser it would be applied to augment the radiotherapy. These studies may pave way for a highly potential targeted therapy for cancer.

Acknowledgements

The authors duly acknowledge the funding support from Department of Science and Technology (Research grant NO: SR/FT/LS-63/2011 and DST–FIST) and Pondicherry University fellowship from UGC (First author). The authors also thank to Central Instrumentation Facility in Pondicherry University.

References

1 E. C. Wang and A. Z. *Wang, Integr. Biol.*, 2014, 6, 9 26.

2 L. Zhang, F. X. Gu, J. M. Chan, A. Z. Wang, R. S. Langer and O. C. Farokhzad, *Clin. Pharmacol. Ther.*, 2008, 83, 761 769.

3 A. Z. Wang, R. Langer and O. C. Farokhzads, *Annu. Rev. Med.*, 2012, 63, 185 198.

4 J. F Lovell, C. S. Jin, E. Huynh, H. Jin, C. Kim, J. L. Rubinstein, W. C. W. Chan, W. Cao, L. V. Wang, and G. Zheng, *Nat. Mater.*, 2011, 10, 324 332.

5 H. M. Xiong, *Adv. Mater.*, 2013, 25, 5329 5335.

6 Y. Zhang, T. R. Nayak, H. Hong and W. Cai, *Curr. Mol. Med.,* 2013, 13, 1633 1645.

7 P. T. Sudheesh Kumar, V. K. Lakshmanan, T. V. Anilkumar, C. Ramya, P. Reshmi, A. G. Unnikrishnan, S. V. Nair and R. Jayakumar, *ACS Appl. Mater. Inter.*, 2012, 4, 2618 2619.

8 B. N Singh, A. K. S Rawat, W. Khan, A. H. Naqvi and B. R. Singh, *PLoS One.*, 2014, 9, e106937.

9 N. Bala, S. Saha, M. Chakraborthy, M. Maiti, S. Das, R. Basu and P. Nandy, *RSC Adv.* 2015, 5, 4993 5003.

10 J. Gupta. P. Bhargava and D. Bahadur, *J. Mater. Chem.B.*, 2015, 3, 1968 1978.

11 H. Duan, D. Wang and Y. Li, *Chem. Soc. Rev.*, 2015, DOI: 10.1039/c4cs00363b.

12 M. Cinelli, S. R. Coles, M. N. Nadagouda, J. Blaszczynski, R. Slowinski, R. S. Varma, and K. Kirwan, *Green Chem.*, 2015, 17, 2825 2839.

13 A. Bharde, D. Rautaray, V. Bansal, A. Ahmad, I. Sarkar, S. M. Yusuf, M.Sanyal and M. Sastry, Small., 2006,2,135 141.

14 N. Pantidos and L.E Horsfall, *J. Nanomed Nanotechnol.*, 2014, 5, 1 10.

15 R. Choi, B. H. Kim, J. Naowaboot, M. Y. Lee, M. R. Hyun, E. J. Cho, E. S. Lee, E.Y. Lee, Y. C. Yang, and C. H. Chun, *Exp. Mol. Med.*, 2011, 43, 676 683.

16 M. Kampa, V. I. Alexaki, G. Notas, A. P. Nifli, A. Nistikaki, A. Hatzoglou, E. Bakogeorgou, E. Kouimtzoglou, G. Blekas, D. Boskou, A. Gravanis and E. Castanas, *Breast Cancer Res*., 2003, 6, R63 – R74.

17 Q. Mu, G. Jiang, L. Chen, H. Zhou, D. Fourches, A. Tropsha, and B. Yan, *Chem. Rev*., 2014, 114, 7740 7781.

18 K. Li, X. Zhao, B. K. Hammer, S. Du and Y. Chen, *ACS Nano*., 2013, 7, 9664 9674.

19 G. Han, N. S. Chari, A. Verma, R. Hong, C. T. Martin and V. M. Rotello, *Bioconjugate Chem*., 2005, 16, 1356 1359.

20 Y. Liu, W. Chen, S. Wang and A. G. Joly, *Appl. Phys. Lett*., 2008, 92, 143901 143903.

21 E. Brun, L. Sanche and C. Sicard-Roselli, *Biointerfaces*., 2009, 72, 128 134.

22 C. D. Kanakis, P. A. Tarantilis, H. A. Tajmir-Riahi, M. G. Polissiou, *DNA and Cell Biol.,* 2007, 26, 63 70

23 J. R. Lakowicz, G. Webber, *Biochemistry*., 1973,12, 4161 4170.

24 S. S. Paul, M. Selim, A. saha and K.K.Mukherjea, *Dalton. Trans.,* 2014, 43, 2835 2848.

25 A. E. Angkawijaya, A. E. Fazary, E. Hernowo, M. Taha and Y. H. Ju, *J. Chem. Eng. Data*., 2011, 56, 532 540.

26 M. Kalinowska, J. Piekut, A. Bruss, C. Follet, J. Sienkiewicz- Gromiuk, R. Swislocka, Z. Rzaczynska and W. Lewandowski, *Spectrochim, Acta Part A. Mol Biomol Spectros*., 2014, 122, 631 638.

27 G. Degrassi, P. Polverino De Laureto and C.V. Bruschi, *Appl. Environ. Microbiol*., 1995, 61, 326 332.

28 S. Meyer, A. Cartelat, I. Moya and Z. G. Cerovic, *J. Exp. Bot*., 2003, 54, 757 769.

29 A. B. Djurisic, W.C. H. Choy, V. A. L. Roy, Y. H. Leung, C. Y. Kwong, K. W. Cheah, T. K. Gundu Rao, W. K. Chan, H. F. Lui and C. Surya, *Adv. Funct. Mater*., 2004, 14, 856 864.

30 T. C. Damen, S. P. S. Porto and B. Tell, *Phys. Rev*., 1965, 142, 570 574**.**

31 J.M. Calleja and M. Cardona, *Phys. Rev*. *B*., 1977, 16, 3753 3761.

32 X. Xue, T. Wang, X. Jiang, J. Jiang, C. Pan and Y. Wu, *Cryst. Eng. Comm*., 2014, 16, 1207 1216.

33 E. Mandak, D. Zhu, T. A. Godany and L. Nystrom, *J. Agric. Food Chem*. 2013, 61, 2446 2452.

34 S. Nagarajan and K. A. Kuppusamy, *J. Nanobiotechnology*., 2013, 11, 11 39.

35 A. Sinhamahapatra, A. K. Giri, P. Pal, S. K. Pahari, H. C. Bajaj and A. B. Panda, *J. Mater. Chem.* 2012, 22, 17227 17235.

36 S. Ma, J. Xue. Y. Zhou, Z. Zhang and X. Wu, *Cryst. Eng.Comm*., 2014, 16, 4478 4484.

37 S. Cho, J. W. Jang, J. S. Lee and K. H. Lee, *Cryst. Eng.Comm.,* 2010, 12, 3929 3935.

38 Y. Kimitsuka, E. Hosono, S. Ueno, H. Zhou and S. Fujihara, *Inorg. Chem*., 2013, 52, 14028 14033.

39 Y. Ni. S. Du and S. Kokot*, Analyst*., 2009, 134, 1840 1847**.**

40 G.Y. Bai, B. Dong. Y.Y. Lu, K.Z. Wang, and L.H. Gao, *J. Inorg. Biochem*., 2004, 98, 2011 2015.

41 S. Supriya and S. Pranab , *Phy.Chem.Chem.Phys.,* 2014, 16, 15355 15356.

42 Y. Baba, C.L. Beathy, A. Kagemato, and C. Gebelien, vol. 186 of ACS Symposium Series, *ACS*, Washington, DC, USA, 1962.

43 M.S. Matos, J.Hofkens, and M.H. Gehlen, *J. Fluoresc.,* 2008, 18, 821- 826.

44 R. Sayeed Ur, Y. Zahid, H. A. Mohammed, S. Tarique, I. M. Hassan and T. Mohammad. *PLoS One*., 2014, 9, e93913

45 H.Ruina, Xu . Guiqing, J. Xiaoying, X. Zaikum, and Cu. Fengling. *J Biochem Molecular toxicology.,* 2012, 26, 193 198.

46 S. Tarique, R. Sayeed Ur, A. M. Husain, M.I. Hassan and T. Mohammad, *Int. J. Biol. Macromol*., 2015, 73, 9 16 .

47 M. Gopal, M.S. Shahabuddin and R.I. Sanjeev, *Proc. Indian Acad. Sci.* (*Chem. Sci.*), 2002,

114, 6, 687 696

48 A. Ganguly, S. Ghosh and N. Guchhait, *Phys. Chem. Chem. Phys.,* 2015, 17, 6597 6605.

49 K. Nejedly, J. Chladkova, M. Vorlickova, I. Hrabcova and J. Kypr, *J. Nucl. Acids Res*, 2005, 33, e5.

50 X. Qu, J. O. Trent, I. Fokt, W. Priebe and J. B. Chaires, *Proc. Natl, Acad. Sci., U S A*. 2000, 97 12032 12037.

51 C. N. Nsoukpoe -Kossi, A. A. Ouameur, T. Thomas, A. Shirahata, T. J. Thomas and H.A. Tajmir–Riahi, *Biomacromolecules.*, 2008, 9, 2712 2718.

52 M. Banik and T. Basu, *Dalton Trans*., 2014, 43, 3244 3259.

53 M. Aslanoglu, C.J. Isaac, A. Houlton and B.R. Horrocks, *Analyst.*, 2000, 125, 1791 1798.

54 M. D. Abramo, C. L. Castellazzi, M. Orozco and A. Amadei, *J. Phys. Chem. B.*, 2013, 117, 8697 8704.

55 A. Chan, R. Kilkuskie and S. Hanlon, *Biochemistry.*, I979, 18, 84 91.

56 S. Roy, P. U. Maheswari, M. Lutz, A. L. Spek , H. den Dulk, S. Barends, G.P. van Wezel, F. Hartl and J. Reedijk, *Dalton. Trans*., 2009, 48, 10846 10860.

57 A. Wojtala. M. Bonora. D. Malinska, P. Pinton, J. Duszynski and M.R. Wieckowsk., *Methods enzymol.*, 2014, 542, 243-263.

58 B.J. Jin, S.H. Bae, S.Y. Lee and S. Imc, Material science and engineering, 2000, 71, 302 305.

59 M.S. Cooke, M.D. Evans, J. Lunec, Oxidative DNA damage: mechanisms, mutation, and disease, *FASEB J.* 2003, 17, 1195 1121.

Foot notes

Figure 1. Proposed mechanism of ferulic acid assisted synthesis of ZnO NPs

Figure 2. Characterization of ZnONPs: Raman spectrum of ZnONPs (a) before calcination (b) after calcination (500°C for 1 hr).

Figure 3. Functional moieties and crystallinity of ZnONPs: FTIR spectrum of functional moieties of the molecule present on ZnONPs (pellet made along with KBr) (a) before calcination (b) after calcinations (500°C for 1 hr). Crystallinity of ZnONPs were analysed by X-Ray diffractometer (c) before calcination (d) after calcination (500°C for 1 hr) (e) JCPDS 98-006-5172.

Figure 4. SEM micrograph of the prepared ZnONPs (a & b) before calcination (c & d) after calcination (500°C for 1 hr).

Figure 5. Chemical composition of ZnONPs analysed by EDAX (a) before calcination b) after calcination (500°C for 1 hr). Elemental mapping image of ZnONPs (c & d) before calcination (e & f) after calcination.

Figure 6. 3D images for surface morphology and line profile of ZnONPs by atomic force microscope. Before calcinations (a & c), after calcinations (b & d).

565

566 **Figure 7.** UV-Visible absorption spectra and fluorsecence emission spectra of Calf thymus-DNA and
567 ZnONPs (a) UV-Visible absorption spectra of CT-DNA alone (0.1 mM of DNA in 10 mM Tris HCl
568 buffer, pH 7.5 at 25°C) and presence of different concentration of ZnONPs (0 to 70 µg/ml). The arrow
569 shows the changes of spectra upon increasing concentration of complex (1) DNA alone, (2) DNA + 10
570 µg/ml ZnO, (3) DNA + 30 µg/ml ZnONPs, (4) DNA + 50 µg/ml ZnONPs, (5) DNA + 70 µg/ml
571 ZnONPs, **Inset:** plot of 1/ A – A_0 vs 1/ [ZnONPs]. (b) Steady state fluorescence spectra of ZnONPs
572 alone and in presence of various concentration of CT-DNA (0-100 µM). The arrow shows the changes
573 of spectra upon increasing concentration of complex (1) ZnONPs 30 µg/ml, (2) DNA (5 µM) +
574 ZnONPs 30 µg/ml (3) DNA (25 µM) + ZnONPs 30 µg/ml, (5) DNA (50 µM) + ZnONPs 30 µg/ml, (6)
575 DNA (100 µM) + ZnONPs 30 µg/ml, **Inset:** plots of 1-I / I_0 vs 1/ [DNA]. (c) Fluorescence emission
576 spectra of EtBr bound CT- DNA alone and in presence of various concentration of ZnONPs (0 – 50
577 µg/ml). The arrow shows the change of spectra upon increasing concentration of complex (1) EtBr-
578 DNA complex (5µM EtBr + 0.1 mM CT-DNA in Tris HCl buffer, pH 7.5), (2) EtBr-DNA complex +
579 10 µg/ml ZnO, (3) EtBr-DNA complex + 30 µg/ml ZnONPs, (4) EtBr-DNA complex + 50 µg/ml
580 ZnONPs .

581

582 **Figure 8.** Conformational changes and electrochemical properties of CT-DNA and ZnONPs. (a)
583 Conformational changes of CT–DNA alone (0.1 mM in Tris HCl buffer, pH 7.5) and in presence of
584 different concentration of ZnONPs (0 – 90 µg/ml) were analyzed by CD spectroscopy. The arrow
585 shows the change of spectra upon increasing concentration of complex. (1) DNA alone, (2) DNA + 10
586 µg/ml ZnO, (3) DNA + 30 µg/ml ZnONPs, (4) DNA + 50 µg/ml ZnONPs. (b) Electro chemical
587 properties of CT – DNA alone (0.1 mM in Tris HCl buffer, pH 7.5) and various concentration of

588 ZnONPs-DNA complexes were analysed by Cyclic voltammogram. The arrow shows the changes of
589 spectra upon increasing concentration of complex (1) DNA alone, (2) DNA + 10 µg/ml ZnONPs, (3)
590 DNA + 30 µg/ml ZnONPs, (4) DNA + 50 µg/ml ZnONPs

591

592 **Figure 9.** Comparative emission spectrum of radiated and non radiated samples of CT- DNA alone
593 (0.1 mM in Tris HCl buffer, pH 7.5) and DNA – ZnO (0 – 50 µg/ml) complex with 5 µM EtBr, The
594 arrow shows the change of spectra upon increasing concentration of complex (1) DNA + EtBr alone (2)
595 DNA- EtBr + 10 µg/ml ZnONPs (3) DNA- EtBr + 30 µg/ml ZnONPs (4) DNA- EtBr + 50 µg/ml
596 ZnONPs,(5) IR*DNA- EtBr alone (6) IR DNA - ZnONPs (10 µg/ml) + EtBr (7) IR DNA - ZnONPs
597 (30 µg/ml)+ EtBr (8) IR DNA - ZnONPs (50 µg/ml)+ EtBr of ZnONPs.(* IR – irradiated)

598

599 **Figure 10.** Comparative conformation changes of radiated and non-radiated CT-DNA (0.1 mM in Tris
600 HCl buffer, pH 7.5) alone and CT-DNA – ZnONPs (30 µg/ml) complexes were analyzed by circular
601 dichroism spectroscopy.

602

603 **Figure 11.** Photoluminescence spectra of ROS generated by gamma irradiation of CT- DNA (0.1 mM
604 in Tris HCl buffer, pH 7.5) and varying concentration of ZnONPs (0–50 µg/ml) with fluorescent prob
605 DCFDA (5 mM). The arrow shows the change of spectra upon increasing concentration of complex (1)
606 IR DNA alone, (2) IR DNA + 10 µg/ml ZnONPs, (3) IR DNA + 30 µg/ml ZnONPs, (4) IR DNA + 50
607 µg/ml of ZnONPs

608

609

610 **Table 1**. The average size of the particles was determined by Debye–Scherrer formula, D = (0.9λ) / (β
611 case θ) in this equation diameter of crystallites are (D), λ denoted the wavelength of CuKα radiation,
612 θ signifies the Bragg angle, β is full – width at half – maximum in radians (FWHM).

2θ degree	**FWHM (β)**	**d- Spacing (A°)**	**Crystallite Size (nm)**
31.79°	0.274	2.81	52.7
34.44°	0.288	2.6	41.3
36.28°	0.311	2.47	100
47.57°	0.381	1.9	22.3
56.65°	0.264	1.62	36
62.91°	0.350	1.47	37.5
66.44°	0.290	1.40	4.8
68.01°	0.300	1.37	26.7
69.15°	0.320	1.357	13.5
72.62°	0.270	1.30	2.2
77.03°	0.420	1.23	4.3
		Average Size	31 nm

613

614

615

616

617

618

619

Fig. 1

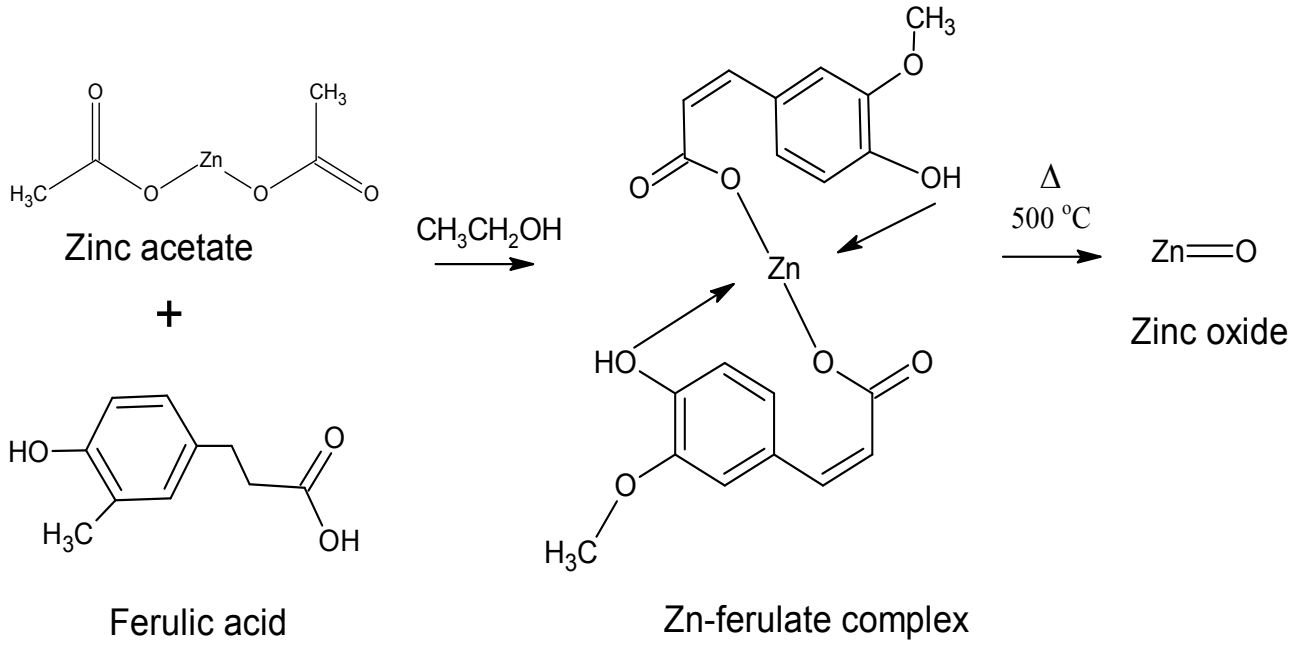

620

621

622

623

624

625

626

627

628

629

630

631

632

633

Fig. 2

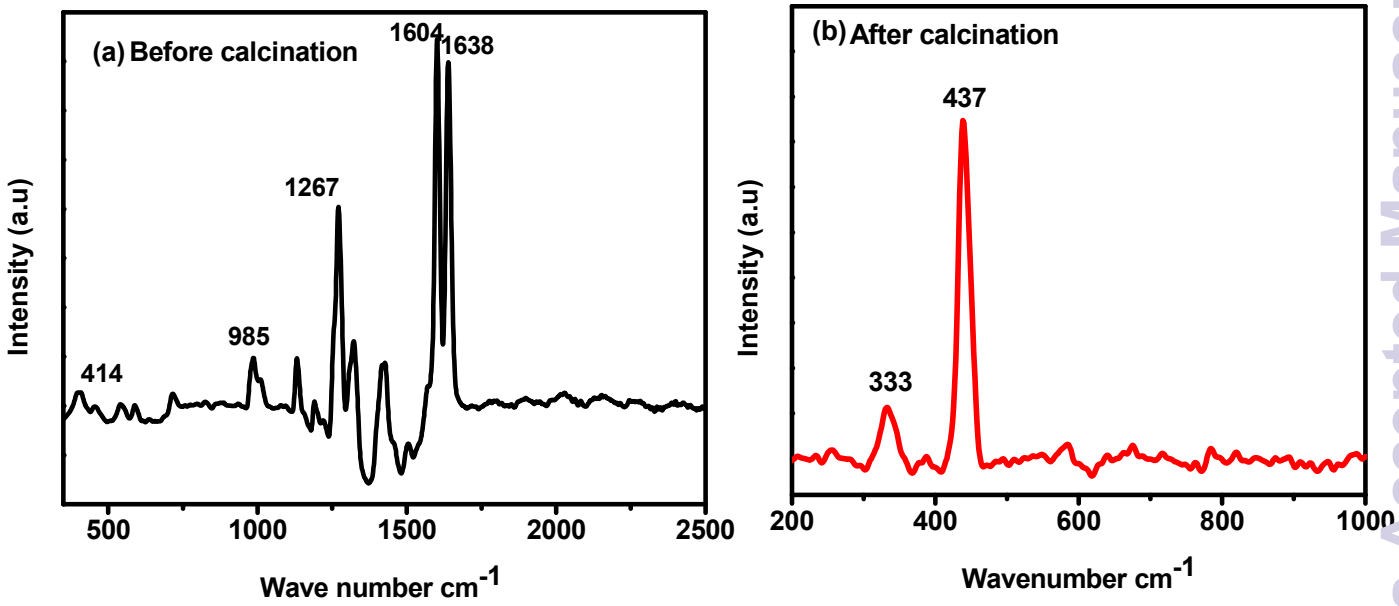

Fig. 3

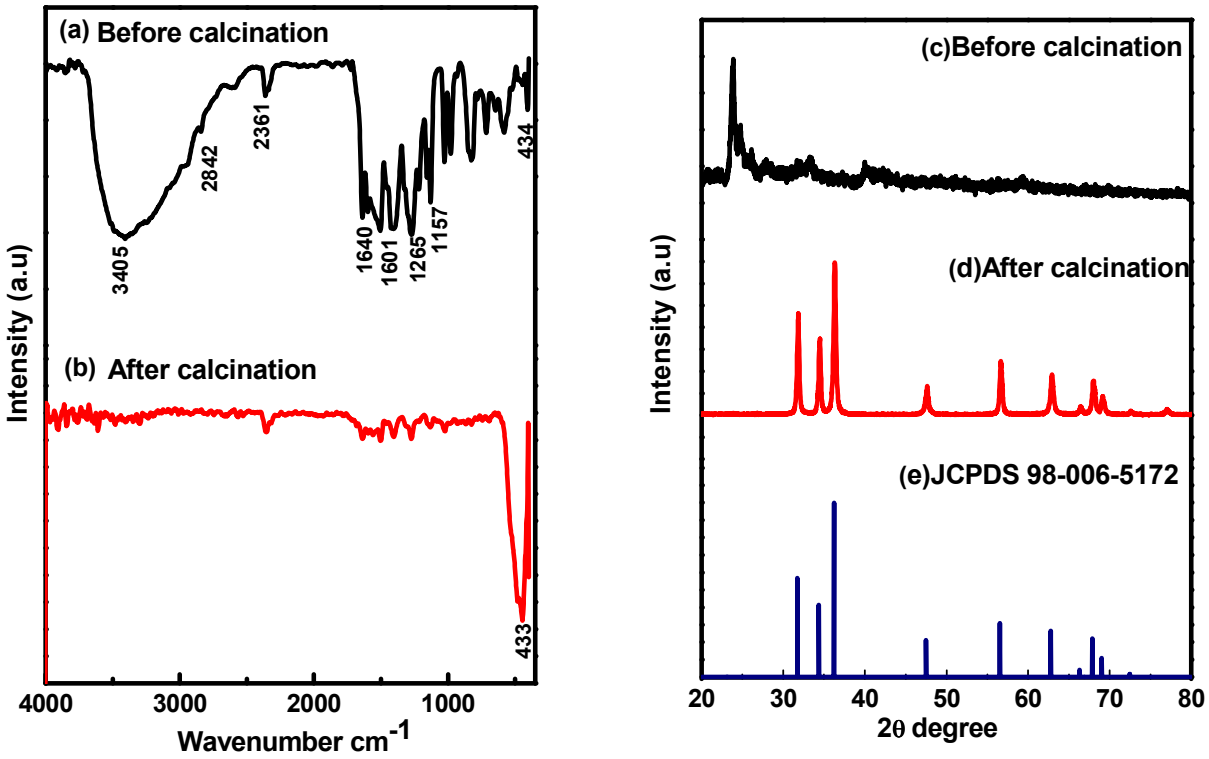

Fig. 4

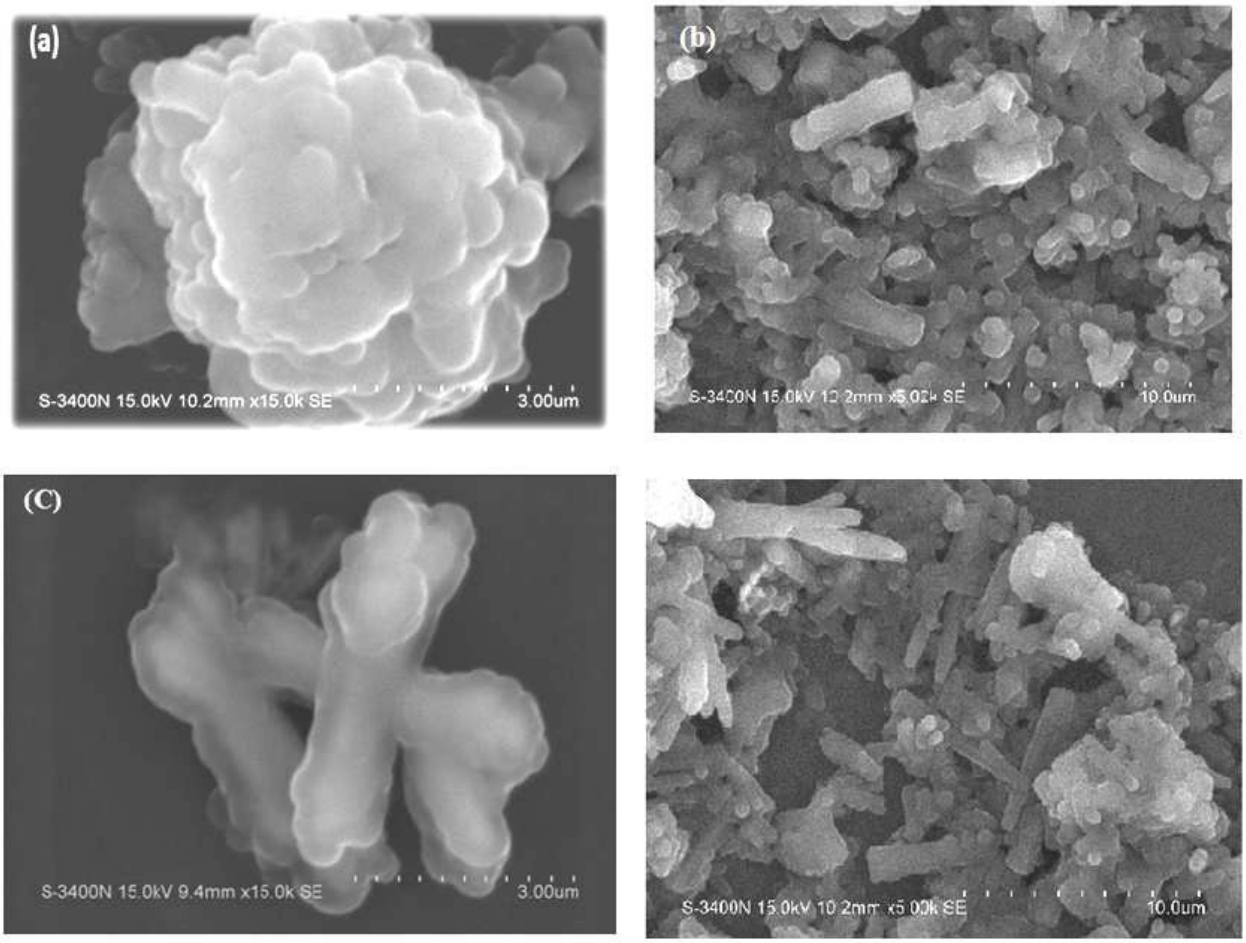

711
712
713
714
715 **Fig. 5**
716
717
718
719
720
721
722
723
724
725
726

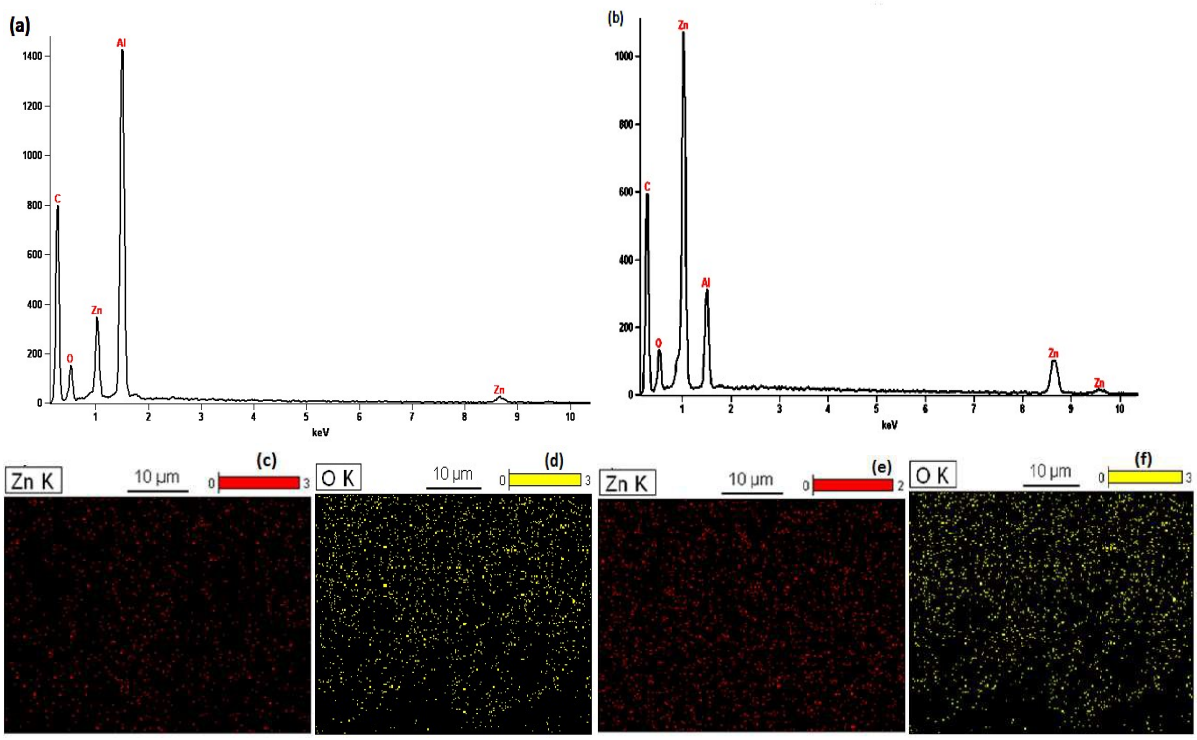

Fig. 6

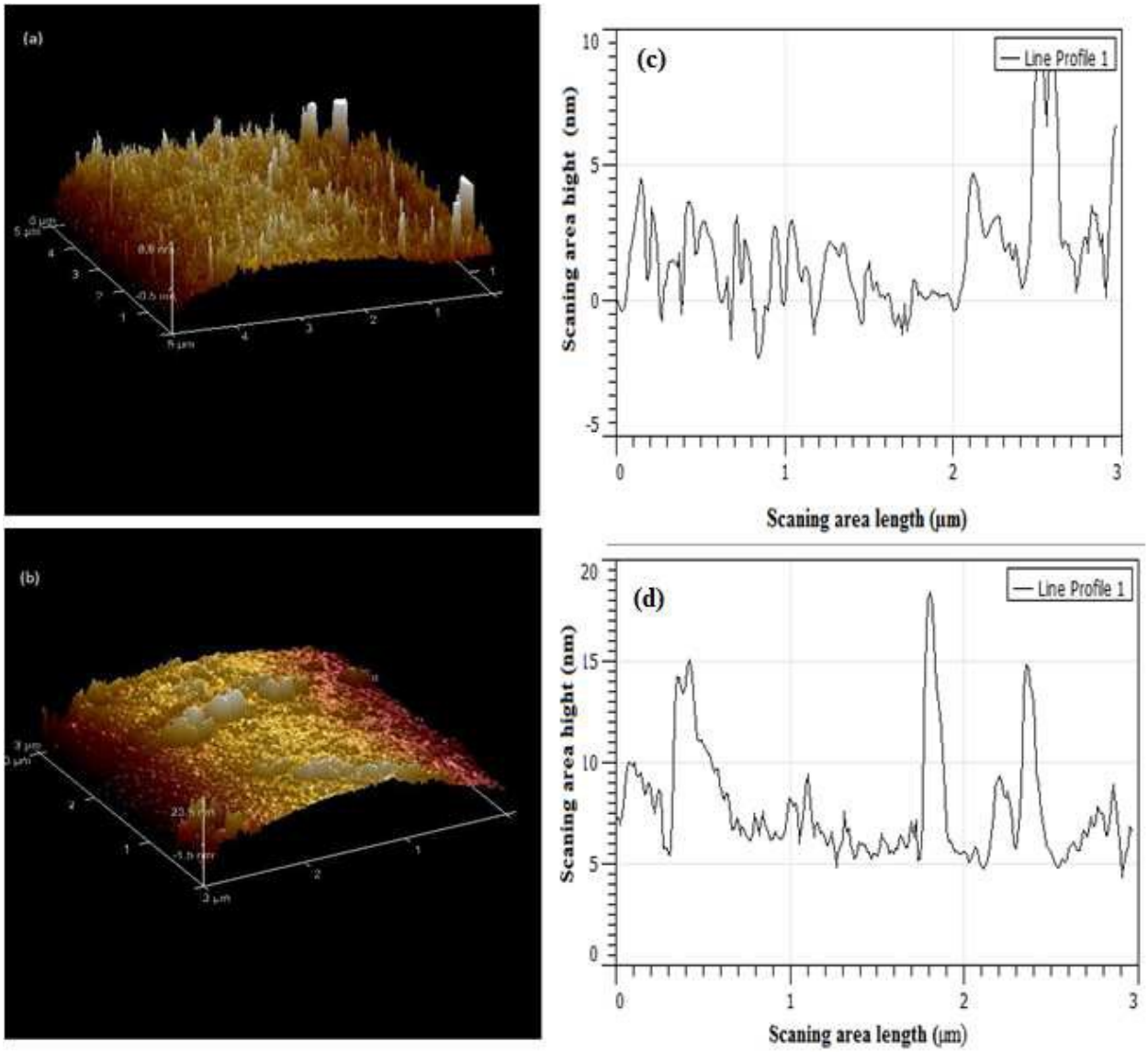

Fig. 7

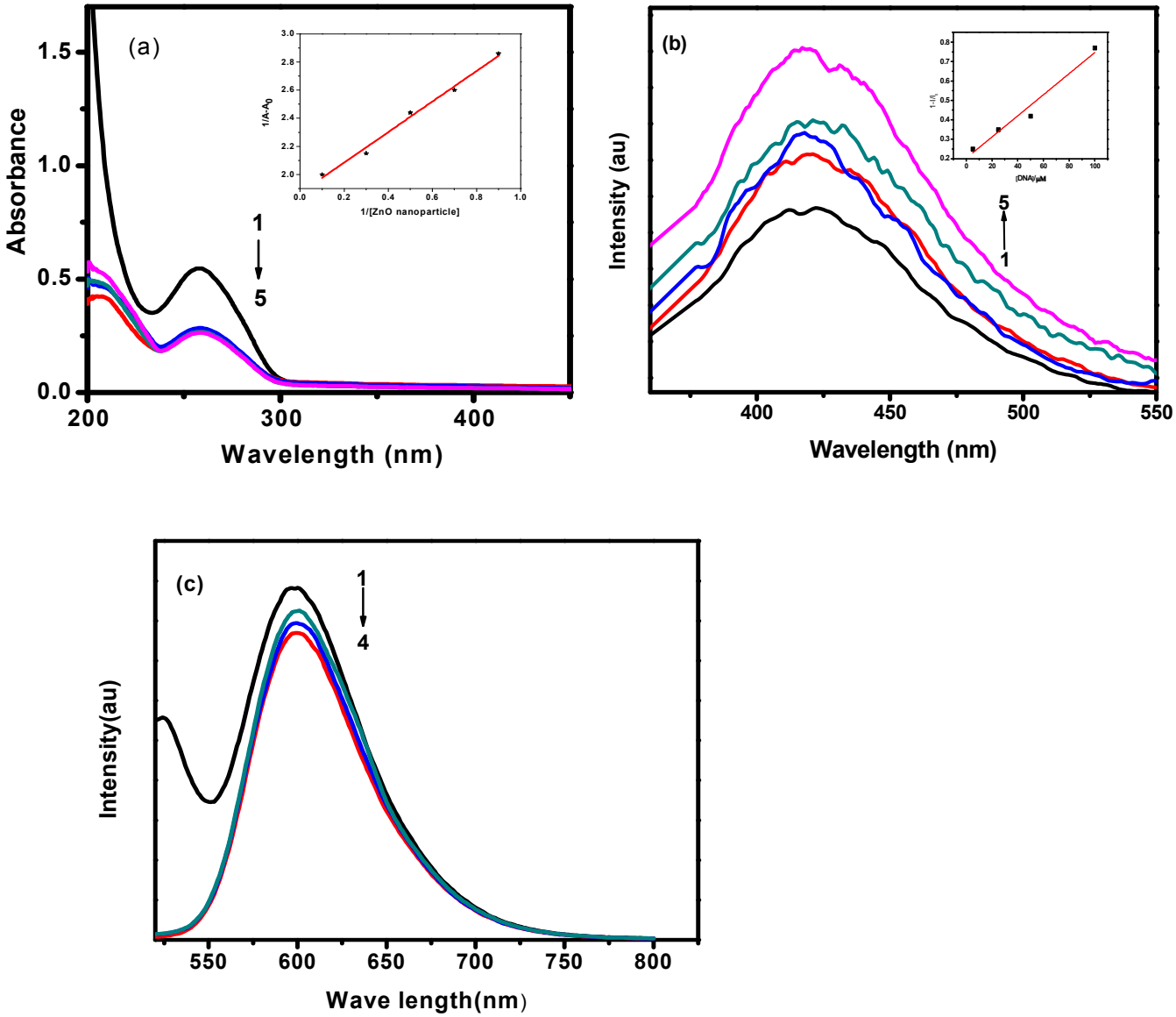

Fig. 8

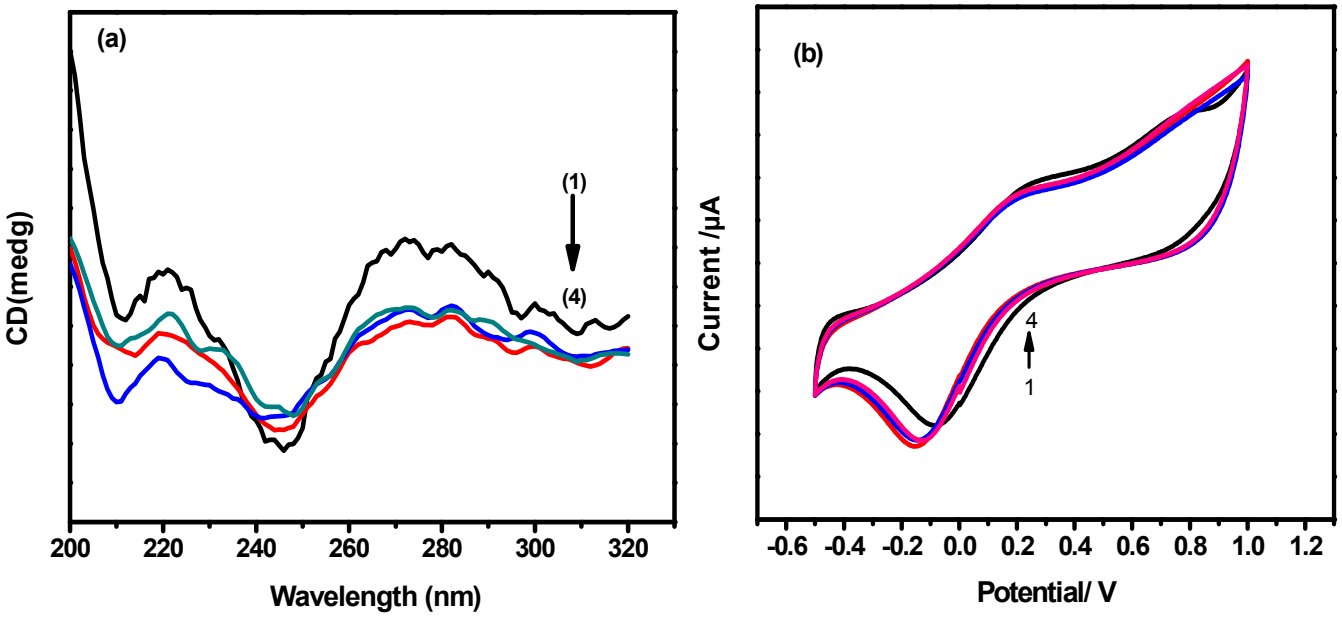

786

787

788

789

790

Fig. 9

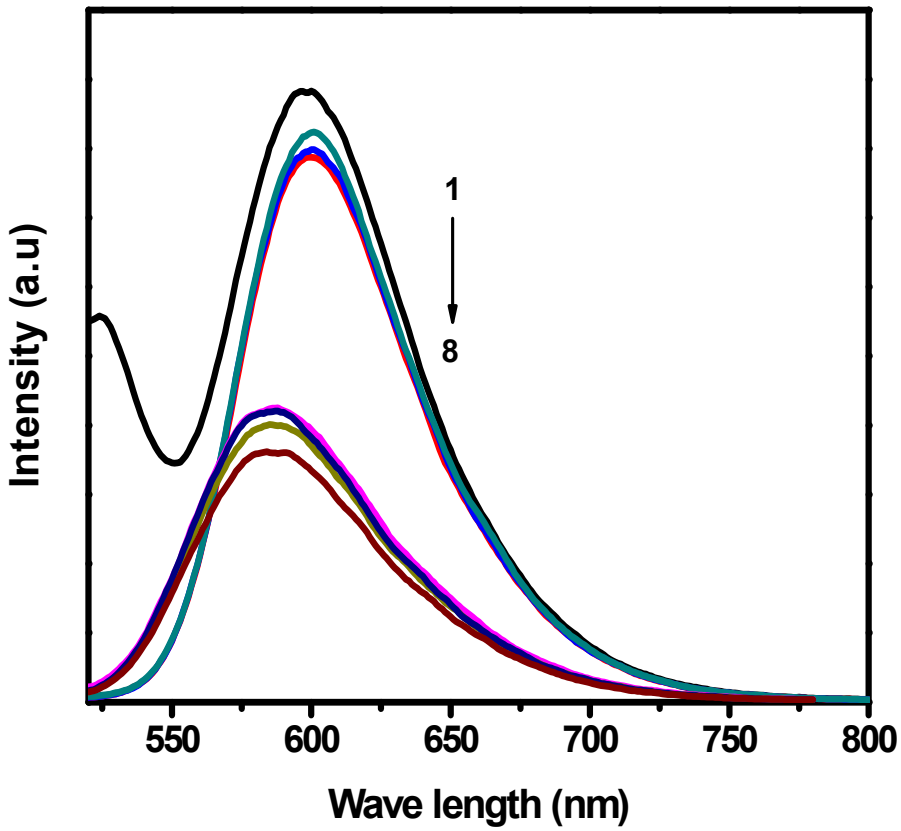

791

792

793

794

795

796

797

798

799

Fig. 10

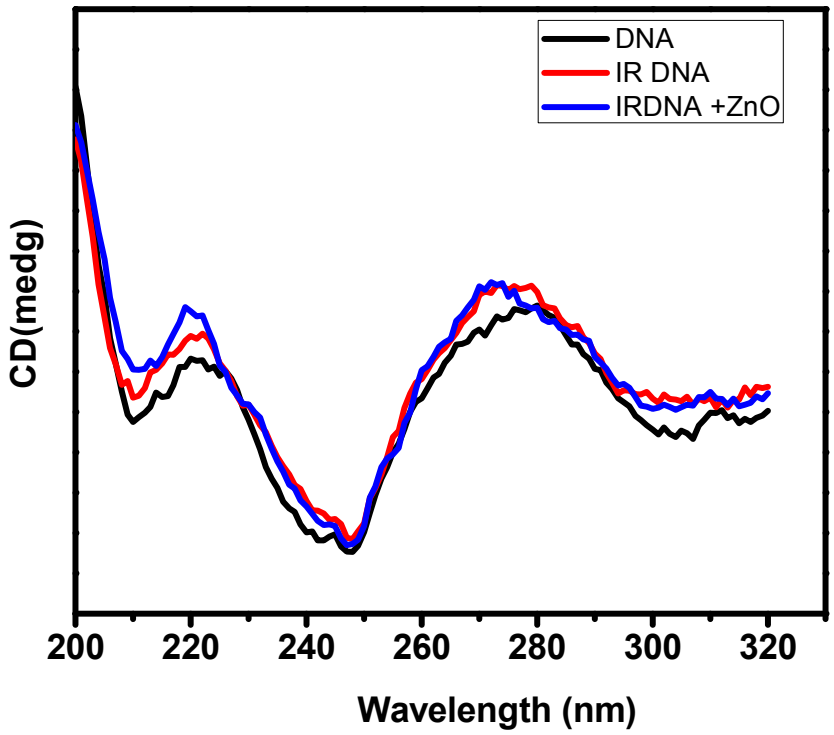

819

820

821

822

823

824

825 **Fig. 11**

826

827

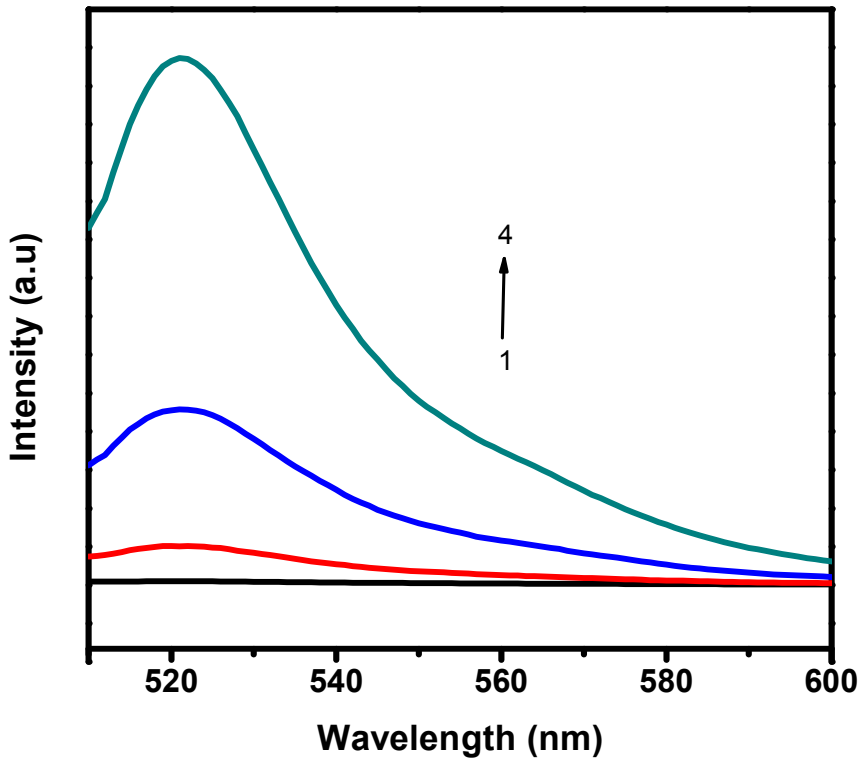

828

829

830

831